analytical chemistry

Article

Cite This: Anal. Chem. 2019, 91, 13675−13680

pubs.acs.org/ac

The BODIPY-Based Chemosensor for Fluorometric/Colorimetric Dual Channel Detection of RDX and PA

Jianmei Gao,[†,§] Xiaoxiao Chen,[‡] Shuqin Chen,[†,§] Hu Meng,[†] Yu Wang,[†] Chunsheng Li,[†] and Liang Feng*[,†]

[†]CAS Key Laboratory of Separation Sciences for Analytical Chemistry, Dalian Institute of Chemical Physics, Chinese Academy of Sciences, Dalian 116023, P. R. China

[‡]Key Laboratory of Radiopharmaceuticals, Ministry of Education, College of Chemistry, Beijing Normal University, Beijing 100875, P. R. China

[§]University of Chinese Academy of Sciences, Beijing 100049, P. R. China

Supporting Information

ABSTRACT: A fluorometric/colorimetric dual-channel chemosensor based on a hydrazine-substituted BODIPY probe has been successfully fabricated for the detection of RDX and PA. The chemosensor displays turn-on fluorescence behavior upon RDX with a detection limit of 85.8 nM, while showing a turn-off response to PA with a detection limit of 0.44 μM. Meanwhile, an obvious color difference is observed by the naked-eye after the reaction for RDX. Thus, in application, a two-to-two logic gate is constructed for potential application in explosives detection. Additionally, portable equipment is also developed for in situ determination of RDX.

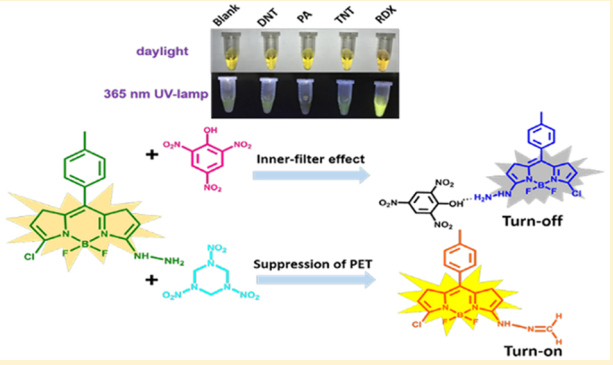

As is known to all, explosives severely endanger global security and the ecological environment.[1,2] Among all the explosives, 1,3,5-trinitroperhydro-1,3,5-triazine (RDX) and picric acid (PA) have been widely applied for both military and civilian use. Although their use is less frequent than that of 2,4,6-trinitrotoluene (TNT), the power index (PI) of these two explosives are much higher (PI_{RDX}: 127%, PI_{PA}: 100%, PI_{TNT}: 89%).[3] In addition, the strong acidity and high water solubility of PA severely threaten the environment.[4,5] Thus, there is an increasing need to develop convenient and effective methods for accurate detection of RDX and PA, not only from a security perspective, but also for human health. Compared with bulky and sophisticated instrumentations, fluorescent and colorimetric chemosensors have obvious advantages such as good portability, low cost, ease of use, etc., and therefore they open up a new way for on-site detection of explosives.[6−8]

Owing to the strong electron-withdrawing groups ($-NO_2$) at an aromatic ring, PA usually can be expediently detected by either colorimetric or fluorometric methods. Numerous optochemical sensors have been developed for PA determination based on conjugated polymers,[9] quantum dots,[10,11] MOFs,[12,13] fluorescent molecular probes,[14−16] and silicon materials.[17] However, RDX does not have typical absorption bands derived from the $\pi-\pi^*$ or n-π^* transition, therefore, only a few methods have been reported to detect RDX by colorimetric means.[18,19] Although several fluorescent chemical sensors have been demonstrated for RDX detection, including nanofiber,[20] small fluorescent probes,[21] conjugated polymers,[22,23] and metal nanoclusters,[24,25] almost all these sensors show a turn-off response, which is easy to be disturbed by interference. A turn-on sensor for RDX with high sensitivity and selectivity is still highly desirable. Furthermore, to the best of our knowledge, an RDX chemosensor with the capability of detecting PA via both fluorescent and colorimetric methods has rarely been reported, which will undoubtedly be more attractive.

Herein, we report a fluorescent/colorimetric dual-channel approach to detect RDX and PA based on a hydrazine-substituted BODIPY (boron-dipyrromethene) probe (named probe **1**). The strong PET effect from hydrazine to BODIPY matrix results in weak emission of probe **1** (about 0.241% compared with quinine sulfate, as given in Supporting Information (SI) Table S1). In the presence of HCHO, which is a major product of RDX decomposition by either alkaline hydrolysis or photolysis,[26,27] electrophilic addition reaction between hydrazine and HCHO takes place, leading to the formation of hydrazone (Scheme 1). Resultantly, the initial intramolecular PET pathway is shut down, and the fluorescence intensity of probe **1** is substantially increasing. Accompanied by a photolysis pretreatment, probe **1** is

Received: June 25, 2019
Accepted: October 10, 2019
Published: October 10, 2019

DOI: 10.1021/acs.analchem.9b02888
Anal. Chem. 2019, 91, 13675−13680

Scheme 1. Photolysis Process of RDX and Response to HCHO of Probe 1, Which Displays Possible Mechanism of Suppression of PET

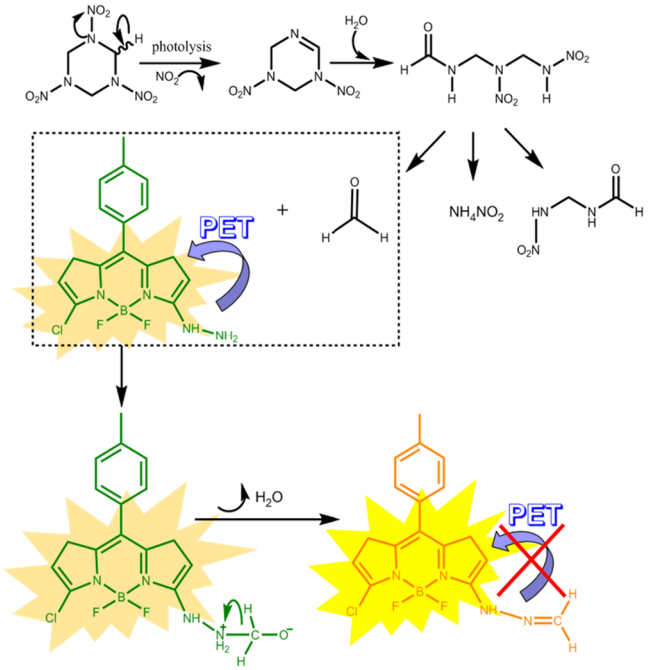

demonstrated to be capable of sensing RDX, even in the presence of most common interferents. Surprisingly, probe **1** is found undergoing an inner-filter course in the presence of PA, resulting in a dramatic fluorescence quenching. Importantly, the color appearance of probe **1** only changes when RDX exists, and remains unchanged in the presence of PA. Compared with other methods, the advantage of this method is shown in SI Table S2. Accordingly, we develop a two-to-two logic gate to realize distinctive detection of RDX and PA based on fluorometric and colorimetric dual channels. Specifically, RDX and PA are regarded as input signals whereas the absorbance and fluorescence intensity of probe **1** represent output signals. The four output combinations (0, 0), (1, 0), (0, 1), (1, 1) allow the direct analysis of RDX and PA. In application, we develop a handhold rapid detector for RDX, which is portable and user-friendly.

EXPERIMENTAL METHODS

Materials and Instrumentation. RDX, PA, 2,4-dinitrotoluene (DNT), and 2,4,6-trinitrotoluene (TNT) standard solutions (1000 μg/mL) were purchased from J&K Scientific Ltd. Other reagents and solvents were of commercial quality and used without further purification. Fluorescence spectra were obtained on a HITACHI F-4600 fluorescence spectrometer. Absorption spectra were determined on a Persee TU-1901 UV−vis spectrophotometer. The pictures of the paper-based sensor were taken by a Nikon D7000 digital camera. ^{1}HNMR spectra were recorded on a JNM-ECZS 400 M spectrometer using tetramethyl silane (TMS) as an internal standard at room temperature and referenced to solvent signals. Mass spectra were obtained on a 6540 UHD Q-TOF mass spectrometer and Bruker Apex IV Fourier Transform mass spectrometer.

Theoretical Calculations. All calculations for explosives (RDX, PA, TNT, DNT) and probe **1** were carried out by the Gaussian 09 program. The structural model for corresponding explosives and probe **1** were optimized using the B3LYP/6-31G(d,p) method, and the related electronic energy levels of HOMO and LUMO orbitals were also obtained by the same method.[28]

Synthesis and Purification of Probe 1. BODIPY-Cl_2 was prepared according to the reported literatures.[29,30] BODIPY-Cl_2 (96 mg, 0.28 mmol) was dissolved in methanol, and about 10-fold hydrazine hydrate was added. After stirring in darkness at room temperature for 12 h, the crude product was obtained via vacuum filtration (see SI Scheme S1). Then, the crude product was purified by column chromatography (dichloromethane: methanol = 60:1 as eluent) to obtain probe **1** as an orange powder (83.5 mg, 87.0%). ^{1}HNMR (400 MHz, $CDCl_3$): δ 7.50 (s, 1H), 7.35 (d, 2H, J = 7.7 Hz), 7.33 (d, 2H, J = 7.7 Hz), 6.89 (d, 1H, J = 4.8 Hz), 6.59 (d, 1H, J = 4.8 Hz), 6.36 (d, 1H, J = 3.8 Hz), 6.18 (d, 1H, J = 3.8 Hz), 4.15 (s, 2H), 2.43 (s, 3H). ESI-MS (m/z): $[M + H]^+$ calcd. $[C_{16}H_{14}BClF_2N_4]^+$, 347.0968; found: 347.1031 (see SI Figures S1 and S2).

Fluorescence Detection of HCHO by Probe 1. 37% formaldehyde solution was diluted to different concentrations (5×10^{-6}, 1×10^{-5}, 5×10^{-5}, 1×10^{-4}, 5×10^{-4}, 7.5×10^{-4}, 1×10^{-3}, 2×10^{-3}, 4×10^{-3}, 6×10^{-3}, 8×10^{-3}, 1×10^{-2}, 2×10^{-2}, 4×10^{-2}, 6×10^{-2}, 8×10^{-2}, and 0.1 M). Ten μL various concentrations of formaldehyde solution were added to 990 μL solution of probe **1** (0.5 mg probe **1** dissolved in 20 mL 80% acetonitrile, acetonitrile: H_2O = 8:2 (V: V)). After incubation for 10 min, fluorescence spectra were measured under 365 nm excitation at room temperature.

Fluorescence Detection of RDX and PA by Probe 1. RDX and PA standard solutions were dried under the flow of N_2, and then they were redissolved in 80% acetonitrile to various concentrations from 0 to 4×10^{-3} M. After that, 10 μL solutions were put in centrifuge tubes and irradiated by a 254 nm UV lamp for 10 min. We added 990 μL of probe **1** in 80% acetonitrile solution to the photolytic solutions. The mixtures were left to stand for 10 min. Finally, the fluorescence emission spectra of the products were recorded under 365 nm excitation at room temperature.

Fabrication of Paper-Based Sensor. RDX, PA, TNT, DNT, and HCl were chosen to test the fluorescent paper-based sensor. First, 2 μL solution of probe **1** (0.5 mg probe **1** dissolved in 20 mL 80% acetonitrile) was dropped onto wax-printed filter paper. After the paper was dried in open air, 1 μL of a different analyte solution (photolysis was required for analytes) was added to the paper. The concentrations of all analytes were 40 μM, and an 80% acetonitrile solution was set as a blank. After drying at room temperature for a few minutes, the pictures of color spots were taken with a camera, and the RGB values as well as brightness of color spots were extracted by Photoshop software.

RESULTS AND DISCUSSION

Design and Synthesis of Probe 1. BODIPY derivatives are excellent candidates as an important class of optical sensors due to their high molar absorption coefficients and fluorescence quantum yields, as well as good chemical stability.[31−33] Thus, we chose BODIPY as a parent molecule, and employed a simple one-step nucleophilic substitution reaction to introduce hydrazine group and obtain probe **1**. The hydrazine group anchored, on the one hand, opened up a new intramolecular PET pathway to BODIPY matrix, and

DOI: 10.1021/acs.analchem.9b02888
Anal. Chem. 2019, 91, 13675−13680

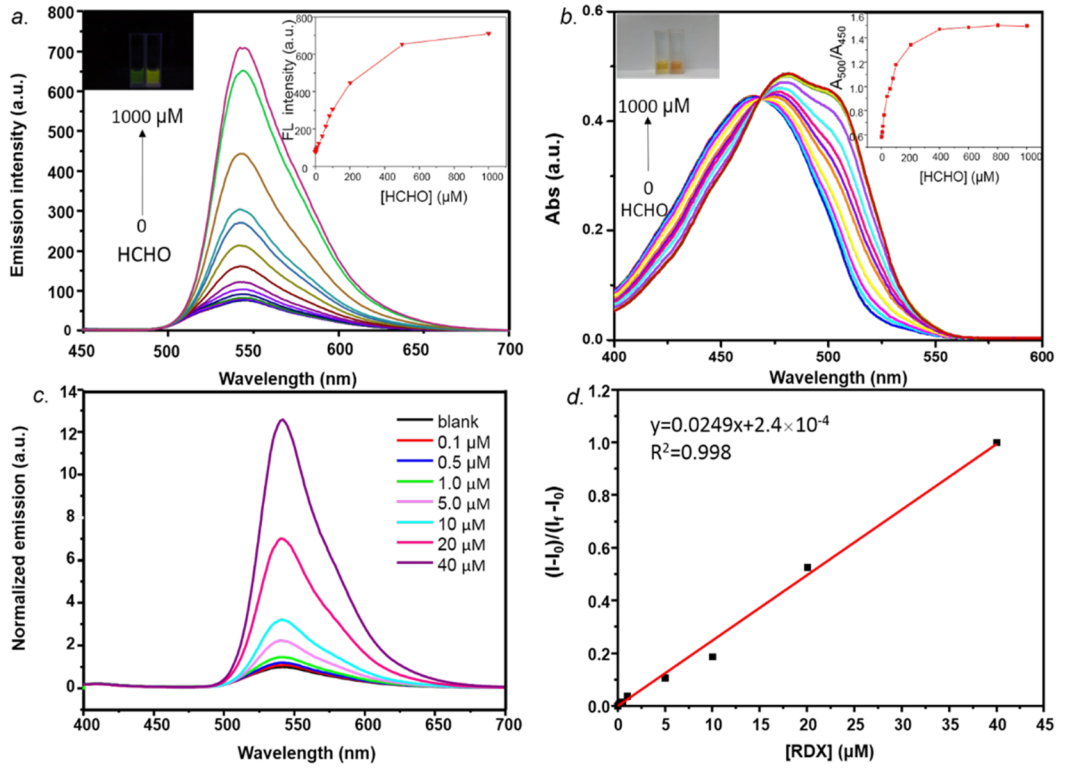

Figure 1. (a) FL emission spectra of products after interaction of probe **1** and HCHO in 80% acetonitrile, λex = 365 nm and λem = 540 nm. Insets show the pictures in the absence and presence of HCHO under 365 nm UV lamp (left), as well as the fluorescence titration fitting curve (right). (b) UV−vis absorption spectra of products after interaction of probe **1** and HCHO in 80% acetonitrile. Inset shows the color change before and after interaction with HCHO in daylight (left), as well as the colorimetric titration fitting curve (right). (c) Normalized emission spectra of products after interaction of probe **1** and photolytic RDX under 254 nm UV lamp. λ ex = 365 nm and λ em = 540 nm. (d) Linear relationship between the growth rate of fluorescence intensity and concentrations of RDX.

dramatically decreased the fluorescent intensity of intrinsic molecule. On the other hand, it endowed the as-synthesized molecule with a reactive site for electrophilic reagent HCHO. The formation of hydrazine was thoroughly characterized by GC-MS and ^{1}H NMR (see SI Figures S3 and S4). Upon the addition of HCHO, under the 365 nm UV excitation, the initial pale yellow-green fluorescence of probe **1** clearly turned to bright yellow (Figure 1a), along with a distinctive color change from yellow to orange (Figure 1b). Literarily, RDX can be decomposed by either alkaline hydrolysis or photolysis,[26,27] and concomitantly yielded HCHO as major degradation product. As such, using probe **1** as a novel RDX sensor seemed applicable if a suitable UV-assisted pretreatment process was involved. Moreover, the unique excitation spectrum of probe **1** was overlapped with absorption of PA, as a result, the determination of PA was possible based on an inner-filter effect. These structural features largely guaranteed the capability of probe **1** in the detection of RDX and PA.

The Detection of RDX in Dual Channel. First, the sensitivity of probe **1** toward RDX was determined. The RDX sample was irradiated by a 254 nm UV lamp for several minutes, then probe **1** was added immediately. As expected, the fluorescence intensity of probe **1** sharply increased within 3 min. In order to evaluate optimal irradiation time, time-resolved control trails were carried out. As shown in SI Figure S5, a dramatic enhancement of fluorescence intensity within 10 min could be observed. However, further extension of irradiation time only gave rise to a negligible enhancement of fluorescent intensity, and thus 10 min was ultimately chosen for preirradiation time. In the titration experiment, by adding photolytic RDX at different concentrations, the fluorescent intensity of probe **1** gradually increased (Figure 1c). By calculation, there was a good linear regression between the growth rate of fluorescent intensity and concentrations of RDX with superior regression coefficient (R^2 = 0.998) in the range of 0−40 μM (Figure 1d), and the limit of detection (LOD) was calculated as low as 85.8 nM based on $3\sigma/k$, where σ is relative standard deviation of blank samples, and k represents the slope of the standard curve, demonstrating the high sensitivity of probe **1** toward RDX. The colorimetric response of probe **1** to photolytic RDX samples was determined as well. The absorption spectrum of the mixture containing probe **1** and 40 μM RDX was almost the same as that of probe **1** and HCHO mixture (see SI Figure S6), which further confirmed that the detection of RDX by probe **1** shared the same mechanism as that of HCHO. This result demonstrated that probe **1** was capable of detecting RDX by both the fluorometric and colorimetric methods.

The Selectivity and the Detection of PA. In order to demonstrate the specific selectivity of probe **1** toward RDX, we first evaluated the interference from common solvent and metal cations, as shown in SI Figures S7 and S8. All experimental procedures were the same as those adopted in RDX detection including prephotolysis of analytes. It was clear that negligible changes in fluorescence intensity were observed in all samples, elucidating the excellent working capability of probe **1**. Then, three explosives were used for further determination, including DNT, PA, and TNT. Upon addition of 40 μM of different explosives to probe **1**, only RDX rendered the fluorescence enhancement to probe **1**, together

DOI: 10.1021/acs.analchem.9b02888
Anal. Chem. 2019, 91, 13675−13680

with an obvious color change (see Figure 2a), indicating the excellent selectivity of probe **1** toward RDX. Interestingly, the

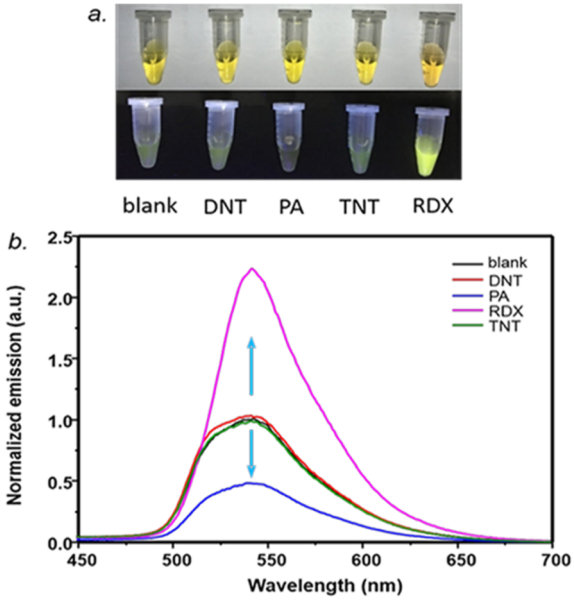

Figure 2. (a) Images of products after reaction of different explosives with probe **1** in daylight (top) and under 365 nm UV lamp (bottom). (b) Normalized emission spectra toward different explosives, the concentration of explosives is 40 Mm, λ ex = 365 nm, and λ em = 540 nm.

addition of PA prominently impaired the fluorescent intensity of probe **1** (see Figure 2b), quenching efficiency in the presence of 40 μM PA is calculated to be 65.14%. However, the fluorescence quenching induced by PA did not reflect its color, indicating probe **1** underwent a totally different sensing mechanism in the presence of PA. By performance of PA titration experiment, the fluorescence intensity of probe **1** declined linearly as the concentration of PA increased from 0 to 40 μM, and the LOD (3σ/k) for PA was calculated as 0.44 μM (see SI Figures S9 and S10). Besides, the distinguishing detection of RDX and PA could be similarly realized by the probe **1**-deposited paper-based analytical device, whose feasibility was certified by principal component analysis (PCA) (see SI Figure S11).

Reaction Mechanism. In order to understand the sensing mechanism of probe **1** toward RDX and PA, we designed several control trials. First, we used H_2O_2 and $K_2S_2O_8$ to exclude the oxidation effect by the thin layer chromatography (TLC) method. An emissive product with the same R_f value presented in the HCHO and RDX groups, as seen in the red circle in SI Figure S12, whereas this product was rarely observed in other groups. It distinctly proved that oxidation effects did not participate in the sensing mechanism. Second, a pH experiment was conducted to exclude the effect of alkylamines generated during photolysis process.[26] As the solution's pH value increased from 4 to 9, adjusted by HCl and NaOH, emission intensity of probe **1** at 520 nm rapidly increased the same as the addition of different alkylamines (see SI Figures S13 and S14). This result was very different from those λ_{emmax} obtained by HCHO or RDX at 540 nm, indicating that FL intensity enhancement at 540 nm was attributed to HCHO rather than alkylamines. It has been reported that NO_2^- was a byproduct as well.[26] With regard to this, we further employed $NaNO_2$ to exclude reactivity of probe **1** toward NO_2^-. Upon addition of 40 μM NO_2^- to the reaction system, fluorescent intensity was unchanged (see SI Figure S15). Accordingly, the electrophilic addition reaction at hydrazine moiety by HCHO produced by photolysis of RDX seemed like the only answer left for sensing mechanism of RDX.

The fluorescence quenching mechanism of probe **1** to PA, was initially assumed originating from strong acidity of PA. However, the pH experiment controlled by HCl unambiguously elucidated that the protonation of probe **1** had almost no effect for FL intensity (as shown in SI Figure S16). Next, FRET behavior between PA and probe **1** was also investigated by UV−vis absorption and fluorescence emission (see SI Figure S17). It could be clearly seen that there was almost no overlap between absorption of PA and emission of probe **1**, which indicated that effective FRET could hardly occur. Then, we utilized theoretical simulations to obtain the highest occupied molecular orbital (HOMO) and lowest unoccupied molecular orbital (LUMO) of probe **1**, RDX, PA, TNT, and DNT.[28] The LUMO (E_{LUMO} = −1.50 eV) level of probe **1** was higher than that of all explosives (see SI Figure S18). That is, if the electron transfer process could happen from LUMO of probe **1** to LUMO of PA, the same process should have occurred for other explosives, but we did not find the same results from TNT or DNT, so electron transfer was not the key reason for the decline of emission intensity. Finally, we tested the above explosives' UV−vis absorptions and probe **1**'s excitation, as well as emission spectrum, which showed apparent overlap between excitation spectrum of probe **1** and absorption of PA (see SI Figure S19). Differently, the absorption spectra of TNT, DNT, and RDX did not overlap with the excitation spectrum of probe **1**. Thus, inner-filter effect of fluorescence was considered to be a vital factor for fluorescence quenching of PA.

Application. Based on the above results, we assumed that probe **1** may serve explosives' detection as a peculiar sensing platform by fluorometric and colorimetric dual detection channels. To prove this assumption, we designed a two-to-two logic gate based on optical response of probe **1** toward RDX and PA. Specifically, the two-to-two decoder converted two input bits into two output bits.[34] Wherein, the presence and absence of RDX (or PA) were defined as "1" and "0" of inputs, respectively, and the FL intensity at 540 nm and absorbance at 500 nm of probe **1** acted as two outputs. The threshold value was set as 60 for FL intensity and 0.62 for absorbance. Once beyond critical value, "1" signal output, otherwise "0" signal output. The logic device is illustrated in Figure 3a, the truth table together with the signal bar chart of FL intensity and absorbance of the two-to-two decoder logic gate are presented in Figure 3b−d. Only the presence of RDX gave rise to the signal "1" in colorimetric channel due to the uniqueness of prominent colorimetric response of probe **1** toward RDX, even in the coexistence of PA. In fluorometric channel, PA played a key role instead, which induced obvious fluorescence quenching and resulted in the output of "0" signal when there was no RDX. The fluorescent intensity of probe **1** at 540 nm could form a logic gate combining NOT and OR to obtain IMP gate,[35] while absorbance at 500 nm acted as a YES gate.

For practical applications, we developed a handheld rapid detector for fluorescent detection of RDX, as shown in Figure 4a. The detector is composed of photolysis light source (265 nm), excitation light source (365 nm), cuvette, convex lenses,

DOI: 10.1021/acs.analchem.9b02888
Anal. Chem. 2019, 91, 13675−13680

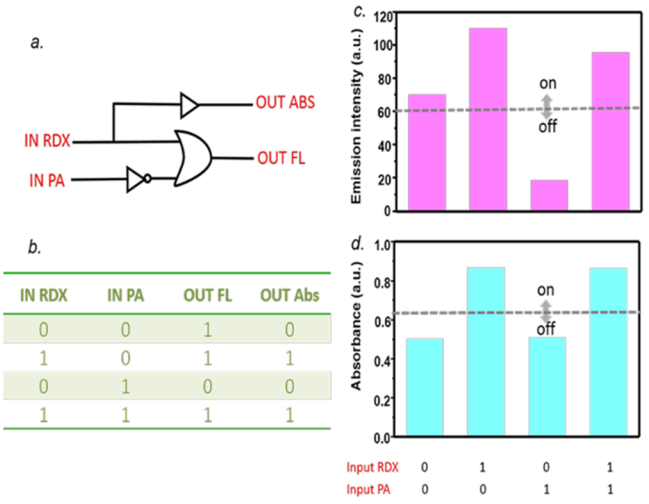

IN RDX	IN PA	OUT FL	OUT Abs
0	0	1	0
1	0	1	1
0	1	0	0
1	1	1	1

Figure 3. (a) The logic device composed of two inputs (RDX and PA) and two outputs (ABS and FL). (b) The truth table for the two-to-two decoder logic gate. (c) The column bars of emission intensity of the logic gate with a threshold of 60. (d) The column bars of absorbance of the logic gate with a threshold of 0.62.

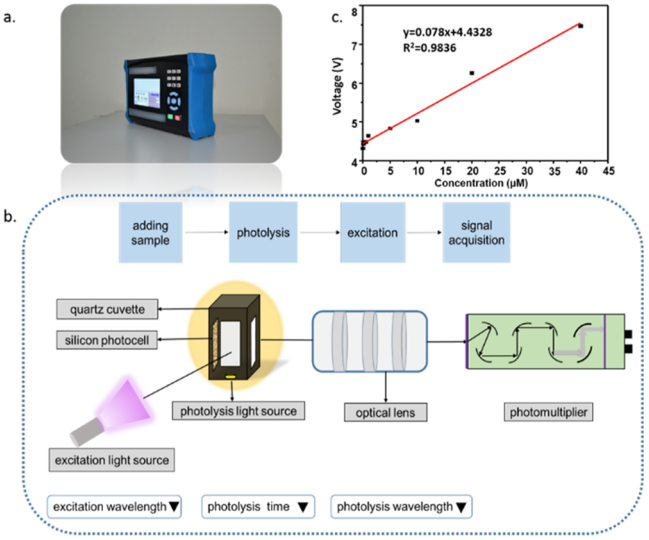

Figure 4. (a) The appearance of equipment established for RDX. (b) Schematic diagram of the equipment. (c) Standard curve obtained by the equipment.

optical filter, and photomultiplier (Figure 4b). The size and interior circuit is demonstrated in SI Figure S20. In use, 20 μL liquid sample was dissolved in 80% acetonitrile aqueous solution and photolyzed for 10 min. We mixed 1980 μL solution of probe **1** with RDX, and the fluorescent intensity was measured after 10 s. The linear regression between fluorescent intensity and concentration of RDX is illustrated in Figure 4c, which exhibits good linearity with a considerable regression coefficient (R^2 = 0.98). This device is portable and user-friendly, providing high potential in practical detection of RDX. (For more details please see SI Figure S21.)

These results elucidated that probe **1** possessed high potential in the distinctive detection of RDX and PA.

CONCLUSION

In summary, we have developed a facile strategy for the determination of RDX and PA using a hydrazine-substituted BODIPY probe (probe **1**) via colorimetric/fluorometric dual channel. After reacting with probe **1**, RDX and PA caused a turn-on and turn-off response in FL intensity, respectively, together with a color change after the reaction for RDX. Taken together, a two-to-two logic gate was constructed, which may emerge as a promising candidate in explosives detection. Furthermore, portable equipment was developed, indicating high potential for practical use for detection of RDX.

ASSOCIATED CONTENT

Supporting Information

The Supporting Information is available free of charge on the ACS Publications website at DOI: 10.1021/acs.analchem.9b02888.

Synthetic procedure of probe **1**, characterizations of probe **1** and products, fluorescence spectra and UV−vis spectra of corresponding products, paper-based sensor, theoretical calculations of explosives, operation procedure of the portable equipment, and other supporting figures and tables (PDF)

AUTHOR INFORMATION

Corresponding Author

*E-mail: fengl@dicp.ac.cn.

ORCID

Liang Feng: 0000-0002-7586-8424

Notes

The authors declare no competing financial interest.

ACKNOWLEDGMENTS

We are grateful for financial support from the STS project (Grant No. KFJ-STS -SCYD −207) from CAS and the National Natural Science Foundation of China (Grant No. 21804132). This paper is dedicated to the 70th anniversary of Dalian Institute of Chemical Physics, CAS.

REFERENCES

(1) Mosca, L.; Karimi Behzad, S.; Anzenbacher, P., Jr. *J. Am. Chem. Soc.* **2015**, *137* (25), 7967−7969.
(2) Peng, Y.; Zhang, A. J.; Dong, M.; Wang, Y. W. *Chem. Commun.* **2011**, *47* (15), 4505−4507.
(3) Türker, L.; Variş, S. *Defence Technology* **2017**, *13* (6), 385−391.
(4) Dinda, D.; Gupta, A.; Shaw, B. K.; Sadhu, S.; Saha, S. K. *ACS Appl. Mater. Interfaces* **2014**, *6* (13), 10722−10728.
(5) Kaur, S.; Bhalla, V.; Vij, V.; Kumar, M. *J. Mater. Chem. C* **2014**, *2* (20), 3936−3941.
(6) Jiang, Y.; Zhao, H.; Zhu, N.; Lin, Y.; Yu, P.; Mao, L. *Angew. Chem., Int. Ed.* **2008**, *47* (45), 8601−8604.
(7) Huang, J.; Gu, J.; Meng, Z.; Jia, X.; Xi, K. *Nanoscale* **2015**, *7* (37), 15413−20.
(8) Dong, M.; Wang, Y. W.; Zhang, A. J.; Peng, Y. *Chem. - Asian J.* **2013**, *8* (6), 1321−1330.
(9) Del Rosso, P. G.; Romagnoli, M. J.; Almassio, M. F.; Barbero, C. A.; Garay, R. O. *Sens. Actuators, B* **2014**, *203*, 612−620.
(10) Dutta, P.; Saikia, D.; Adhikary, N. C.; Sarma, N. S. *ACS Appl. Mater. Interfaces* **2015**, *7* (44), 24778−24790.
(11) Lin, L.; Rong, M.; Lu, S.; Song, X.; Zhong, Y.; Yan, J.; Wang, Y.; Chen, X. *Nanoscale* **2015**, *7* (5), 1872−1878.
(12) Yingli, Hu; Meili, Ding; Xiao-Qin, Liu; Lin-Bing, Sun; Jiang, H.-L. *Chem. Commun.* **2016**, *52*, 5734−5737.
(13) Gao, Y.; Qi, Y.; Zhao, K.; Wen, Q.; Shen, J.; Qiu, L.; Mou, W. *Sens. Actuators, B* **2018**, *257*, 553−560.
(14) Yogesh, Erande; Santosh, Chemate; Ankush, More; Sekar, N. *RSC Adv.* **2015**, *5*, 89482−89487.

DOI: 10.1021/acs.analchem.9b02888
Anal. Chem. 2019, 91, 13675−13680

(15) Pandith, A.; Kumar, A.; Lee, J.-Y.; Kim, H.-S. *Tetrahedron Lett.* **2015**, *56* (51), 7094−7099.
(16) Govindasamy, Sathiyan; Sakthivel, P. *RSC Adv.* **2016**, *6*, 106705−106715.
(17) Han, Y.; Chen, Y.; Feng, J.; Liu, J.; Ma, S.; Chen, X. *Anal. Chem.* **2017**, *89* (5), 3001−3008.
(18) He, Y.; Wang, L. *J. Hazard. Mater.* **2017**, *329*, 249−254.
(19) Uzer, A.; Can, Z.; Akin, I.; Ercag, E.; Apak, R. *Anal. Chem.* **2014**, *86* (1), 351−356.
(20) Xiong, W.; Liu, X.; Wang, T.; Zhang, Y.; Che, Y.; Zhao, J. *Anal. Chem.* **2016**, *88* (22), 10826−10830.
(21) Wang, C.; Huang, H.; Bunes, B. R.; Wu, N.; Xu, M.; Yang, X.; Yu, L.; Zang, L. *Sci. Rep.* **2016**, *6*, 25015−25023.
(22) Gopalakrishnan, D.; Dichtel, W. R. *J. Am. Chem. Soc.* **2013**, *135* (22), 8357−8362.
(23) Gopalakrishnan, D.; Dichtel, W. R. *Chem. Mater.* **2015**, *27* (11), 3813−3816.
(24) Enkin, N.; Sharon, E.; Golub, E.; Willner, I. *Nano Lett.* **2014**, *14* (8), 4918−4922.
(25) Essner, J. B.; Chen, X.; Wood, T. D.; Baker, G. A. *Analyst* **2018**, *143* (5), 1036−1041.
(26) Vimal, K. Balakrishnan; Annamariahalasz; Jalal, Hawari *Environ. Sci. Technol.* **2003**, *37*, 1838−1843.
(27) Hawari, J.; Halasz, A.; Groom, C.; Deschamps, S.; Paquet, L.; Beaulieu, C.; Corriveau, A. *Environ. Sci. Technol.* **2002**, *36*, 5117−5123.
(28) Ju, B.; Wang, Y.; Zhang, Y. M.; Zhang, T.; Liu, Z.; Li, M.; Xiao-An Zhang, S. *ACS Appl. Mater. Interfaces* **2018**, *10* (15), 13040−13047.
(29) Mukulesh, Baruah; Wenwu Qin, N. B.; Wim, M. De Borggraeve; Boens, N. l. *J. Org. Chem.* **2005**, *70*, 4152−4157.
(30) Dylan, W. Domaille; Li, Zeng; Chang, C. J. *J. Am. Chem. Soc.* **2010**, *132*, 1194−1195.
(31) Kobayashi, T.; Komatsu, T.; Kamiya, M.; Campos, C.; Gonzalez-Gaitan, M.; Terai, T.; Hanaoka, K.; Nagano, T.; Urano, Y. *J. Am. Chem. Soc.* **2012**, *134* (27), 11153−11160.
(32) Ulrich, G.; Ziessel, R.; Harriman, A. *Angew. Chem., Int. Ed.* **2008**, *47* (7), 1184−1201.
(33) Jia, M. Y.; Niu, L. Y.; Zhang, Y.; Yang, Q. Z.; Tung, C. H.; Guan, Y. F.; Feng, L. *ACS Appl. Mater. Interfaces* **2015**, *7* (10), 5907−5914.
(34) Xu, X. Y.; Lian, X.; Hao, J. N.; Zhang, C.; Yan, B. A double-stimuli-responsive fluorescent center for monitoring of food spoilage based on dye covalently modified EuMOFs: From sensory hydrogels to logic devices. *Adv. Mater.* **2017**, *29* (37).1702298
(35) Liu, J.; He, X.; Zhang, J.; He, T.; Huang, L.; Shen, J.; Li, D.; Qiu, H.; Yin, S. *Sens. Actuators, B* **2015**, *208*, 538−545.

DOI: 10.1021/acs.analchem.9b02888
Anal. Chem. 2019, 91, 13675−13680